Dynamic Topology of Fullerene Coalescence

Yufeng Zhao, Boris I. Yakobson,* and Richard E. Smalley
Center for Nanoscale Science and Technology, Rice University, Houston, Texas 77005
(Received 11 January 2002; published 18 April 2002)

Atomic rearrangements leading to the coalescence of fullerene cages are revealed by topological analysis. Paths found for nanotubes and C_{60} consist exclusively of Stone-Wales bond rotations. Computed intermediate states show gradual evolution from separate clusters to completely fused coherent units. Molecular dynamics simulations follow the predicted routes, overcome the nucleation barrier, and reach a final annealed state. While the overall behavior resembles macroscopic sintering, the nanoscale neck undergoes quantized changes in diameter and crystalline order.

DOI: 10.1103/PhysRevLett.88.185501 PACS numbers: 61.46.+w, 81.07.–b

Fusion of smaller components into a larger whole is a ubiquitous process in condensed matter. At the molecular scale it corresponds to chemical synthesis, where the exact rearrangement of atoms can be recognized. Coalescence or sintering of macroscopic parts is usually driven by well-defined thermodynamic forces (frequently, surface energy reduction), but the atomic evolution paths are so numerous that their exact identification is irrelevant. Exploring the possibility of two particles merging with atomic precision becomes compelling at the nanometer scale, where one aspires to "arrange the atoms one by one" [1]. Are the initial and final states connected by a feasible path of atomic movements, or separated by insurmountable barriers? Direct molecular dynamics (MD) investigations are usually hampered by energy landscape traps, and beyond very few atomic steps need to be augmented with additional analysis [2].

An example of very small particles is offered by fullerene cages and carbon nanotubes (CNTs) both being the subjects of recent studies [3]. Fusion of fullerenes has been reported [4,5] and the lateral merging (diameter doubling) of CNTs has been observed and simulated [6]. In contrast, head-to-head CNT coalescence remains unexplored and of particular theoretical and practical interest: Is it permitted by topology rules to eliminate all the pentagons present in the CNT ends, and thus dissolve the caps completely? Can this occur through a series of well-defined elementary steps, and what is the overall energy change if the system evolves through intermediate disordered states to the final hexagonal lattice of a continuous tubule? If feasible, such "welding" can lead to an increase of connectivity in CNT arrays in bundles/ropes and crystals, and thus to detectable improvement in mechanical, thermal, and electrical material properties. In addition, determining the paths of tube coalescence can shed light on the underlying mechanism of recently reported condensed phase conversion [7] and CNT crystal synthesis [8] from C_{60} components.

In the following, we first present an explicit topological transformation sequence, and describe the guiding principles of its derivation. Then the energies of the series of intermediate configurations are computed, in order to evaluate the physical accessibility of the final minimum. Molecular dynamics simulations follow, to show the role of configurational entropy at high temperatures. Finally, we discuss the physical consequences of the proposed head-to-head coalescence, how it can be facilitated in experiment, and the possible implications for CNT synthesis.

The answer to the questions posed above is essentially a proof of existence by construction (Figs. 1, 2, and 4, below). The derivation has been assisted by the projection method [9] and a few guiding principles. First, only low-energy gradual transformations are of interest (not high-energy fragmentation and rebuilding as in the graphite ablation for fullerene synthesis), as in a continuous scenario of an emerging and widening neck,

Second, such gradual "morphing" must be achieved through atomic steps of low energy, avoiding wherever possible dangling bonds, vacancies, or interstitials. Studies of fullerene isomerization [2,10] and relaxation in nanotubes [11] indicate that the lowest barrier step is a single bond flip rotation of "pyracylene" or Stone-Wales (SW) type [3,10]. This leads to an even more taxing question: Can the fusion occur by exclusively a sequence of SW steps? (Surprisingly, the answer is positive, as shown below.) Third, we seek the lowest energy path among the SW routes and must avoid highly distorted polygons below pentagons or above heptagons, and keep the number of these low. A painstaking analysis reveals the routes for several archetypal tube types.

The steps can be examined in a geodesic projection (Fig. 1, left), where the caps are stretched in order to flatten the map, but preserve the exact topology of the 3D structures (Fig. 1, right). The top and bottom halves of the snapshot 1a correspond to the separate caps, so that the two horizontal lines in the middle are the apex pentagons. In particular, Fig. 1a shows two $(5, 5)$ tubes facing in a staggered fashion, with the apex pentagons misoriented by $\pi/5$. Only the initial transition from these disconnected manifolds (Fig. 1a) to a single continuous network inevitably involves out-of-plane atomic excursions and the formation of new bonds (Fig. 1b), similar to

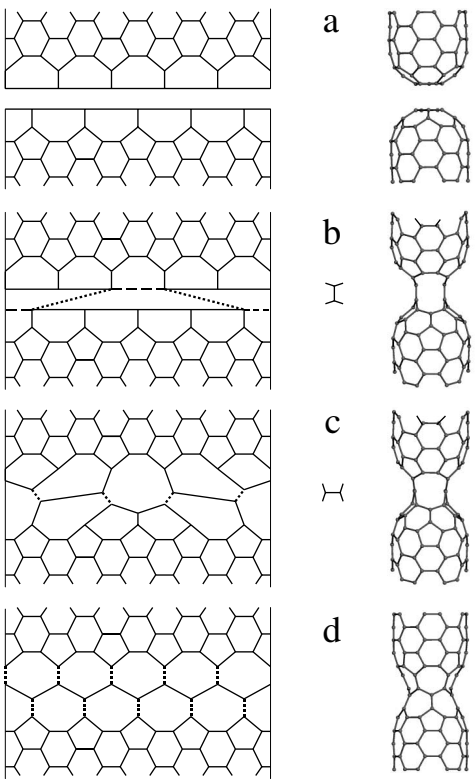

FIG. 1. 2D geodesic projection (left) and the actual 3D structures (right) show the transformations from a pair of separate (5,5) tubes (a) to a single defect-free CNT. Primary "polymerization" links form as two other bonds break [(b), dashed lines]. The $\pi/2$ rotations of the links (hereafter the bonds subject to such SW flips are dotted) and the SW flips of the four other bonds in (c) produce a (5,0) neck (d). It widens by means of another ten SW rotations, forming a perfect single (5,5) tubule (not shown).

C_{60} polymerization [12]. The incurred sp^3 hybridization is not too costly and is eliminated at once by the breaking of adjacent bonds in the original network. The next two identical steps are already SW flips rotating the link bonds from the axial (vertical) to the circumferential (horizontal) direction (Figs. 1b and 1c). The caps become connected by two H-shaped bridges, with the heptagons at the top and bottom and larger polygonal holes on the sides (Fig. 1c). Further, four identical SW flips (bonds marked in Fig. 1c) follow in a zigzag order along the circumference, eliminating the larger polygons and producing a more regular all-heptagon belt (Fig. 1d). One can recognize a very short (5,0) neck connecting the initial (5,5) tubes. Finally, SW rotations of the marked bonds in circumferential order transform all heptagons (and the adjacent pentagons) into a hexagonal lattice, the neck widens into a perfect single (5,5) CNT, and completes the coalescence. A sequence on the right of Fig. 1 shows the corresponding actual relaxed 3D configurations. The overall hourglass shape change resembles macroscopic sintering, but is achieved here exclusively by recurring bond rotations within the two-dimensional membrane.

We now turn to the coalescence of the common (10,10) CNTs (Fig. 2) [13]. Analysis of these larger cages demonstrates the scalability of the mechanism, whose main features remain similar for different CNTs. Indeed, initial cap bonding, formation of the smallest (5,0) neck, and its widening into a (5,5) neck (Fig. 2b) can follow the same path described above for the (5,5) + (5,5) case. From this point further rounds of SW flips (bonds marked in Figs. 2b–2d) occur in circumferential order and gradually widen the neck to the final (10,10) size. Remarkably, at this late stage in Fig. 2d the distinct 5/7 edge dislocation cores can be recognized. As relaxation continues, these dislocation pairs glide to meet and annihilate, $5/7 + 7/5 \rightarrow 5/7/7/5 \rightarrow 0$, all via SW flips only. This completes the coalescence in the theoretical construction, as is also observed in our hands-off MD simulation, and is exactly the reverse of the emergence, split, and glide apart of the 5/7 pairs in the relaxation under high tension [11]. Elimination of the last series of 5/7 defects corresponds to the annealing of tilt boundaries between the lattice grains

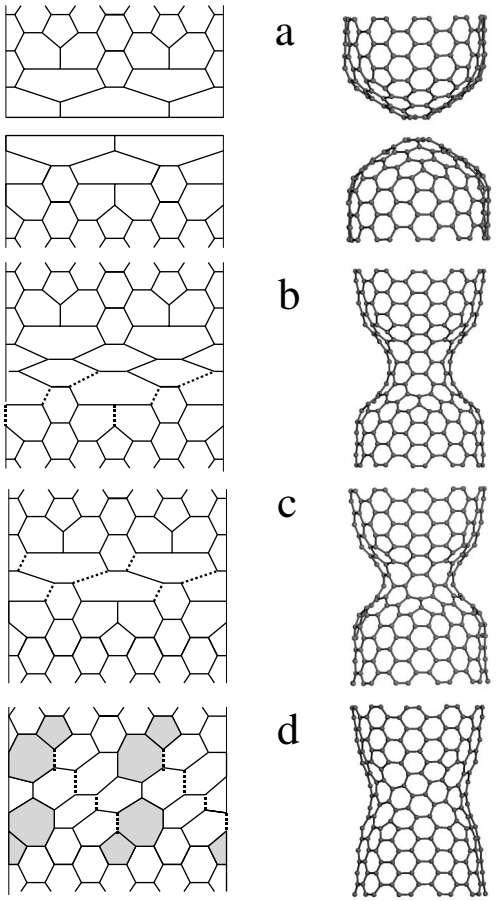

FIG. 2. 2D-projections (left) and the computed 3D intermediate structures (right) in the coalescence of the two (10,10) CNTs: separate caps (a) in a sequence similar to Fig. 1 develop a (5,5) junction (b), which then shortens (c) and widens (d) into a (10,5) neck. Glide of the shaded 5/7 dislocations completes the annealing into a perfect (10,10) CNT (not shown). Because of the fivefold symmetry, only two cells are displayed [13].

of different orientations, i.e., different chirality: (10, 10) next to (10, 5) next to another (10, 10) (Fig. 2d). Neck formation and growth is general in sintering, but the diameter of the nanoscale junction is quantized as it undergoes the transformations $(5,0) \rightarrow (5,5) \rightarrow (10,5) \rightarrow (10,10)$, a perfect cylinder. We have similarly analyzed coalescence of the zigzag (15, 0) pair and some other CNTs. The evidence suggests that the revealed scenario is rather robust, although a general proof may present an arduous task for polyhedral topology.

The paths found by inspection are not unique. We evaluate their feasibility for actual high temperature coalescence by calculating the energies of intermediate structures, and performing MD simulations. Figure 3 shows the results of full relaxation for each of the isomers numbered from the initial separate cage configurations along the paths (essentially the number of SW steps). All energies are computed within a tight binding (TB) approximation [14] and some are verified with density functional *ab initio* methods [15]. Overall the dependencies resemble nucleation in a phase transition, with a barrier followed by reduction in energy upon completion. Structures shown in the figures are for the lowest energy routes found. The path for the (10, 10) pair is the longest, as reconstruction of the wider neck requires 68 steps. It has the highest barrier, near 8 eV, followed by a total energy reduction of 27 eV. A (5, 5) pair annealing into a single tube requires 18 steps, has a barrier of 3.7 eV and is exothermic by 14 eV. Linear slopes at the late stage of coalescence correspond to dislocation pairs gliding down the attraction potential [16] followed by annihilation.

Another important [7,8] case involves merging a C_{60} cage to the (10, 10) tube. A sequence of 2D maps is shown in Fig. 4, left. Again, there exists a SW path of 63 steps that can be divided into two stages [13]. First, the cap bonding followed by the (5, 5) collar formation in Figs. 4b can go on exactly as in the (5, 5) + (5, 5) fusion. Further bond flips are shown in Figs. 4b and 4c. The SW sequence marked in Fig. 4c leads to a complete C_{60} dissolution in the CNT, which thus accrues new material and increases in length by one and one-half lattice parameter (0.367 nm. Notably, the structure of the cap is completely restored, and the process can recur as the next C_{60} arrives, $C_n + C_{60} \rightarrow C_{n+60}$, etc., in Fig. 4, right. This reaction releases 22 eV of heat [0.4 eV per atom, in accordance with binding energies in C_{60} and in (10, 10) CNT], preceded by the coalescence barrier 4.3 eV (Fig. 3).

Classical potential [17] MD generally follows the theoretical paths. Simulations even at 3 000 K are excessively long, because the system does not evolve unidirectionally but rather undergoes random walk returns and retries [13]. Similar to sintering, the process is facilitated by axial compression ($f \sim 1 - 10$ nN), as the energy is replaced by the enthalpy, $E + fl$. This agrees with the gradual length reduction by $\Delta l \sim 3$ Å when the covalent bonds and the neck form. The ideal and MD paths can be compared by matching the configurations of similar shapes, used as a "degree of transformation." Sample snapshots were relaxed to the local minima with zero kinetic and elastic energy. Plotted in Fig. 3 the MD results (TB) are somewhat higher than for the ideal route, reflecting a few extra

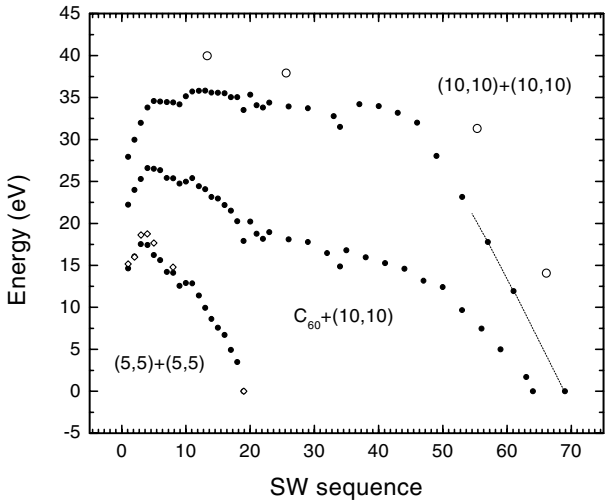

FIG. 3. Energies of metastable structures along the coalescence paths for (5, 5) + (5, 5), (10, 10) + (10, 10), and C_{60} + (10, 10), plotted as functions of the number in the SW sequence (TB approximation, solid circles). Also shown are test points of *ab initio* relaxation (open squares) and several sample structures obtained in high temperature MD (open circles).

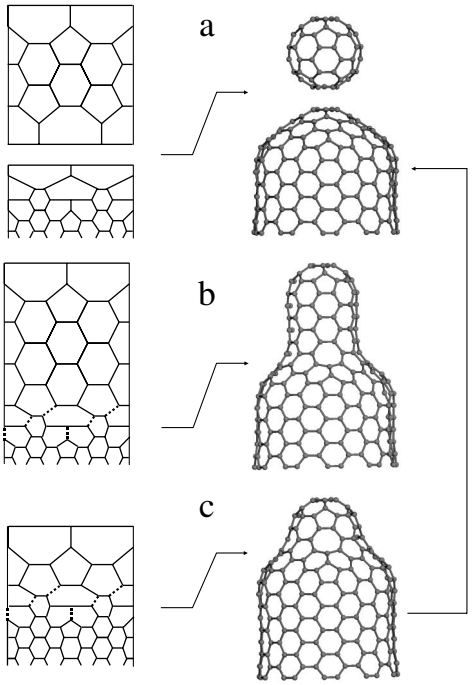

FIG. 4. C_{60} and a (10, 10) tube (a) can fuse by first building a (5, 5) junction (b) through the same steps as shown in Fig. 1. SW flips of the bonds indicated in (b) shorten the neck, and after two such rounds it transforms into (c). Continuing the SW steps in (c) completely dissolves the C_{60} bulge forming a longer (10,10) tubule with the restored perfect cap that permits further fusion processes [13].

SW defects or irregular polygons present in the high temperature path. However these defects are annealed in the final state. Annihilation of $5/7$'s in the concluding stage of coalescence (reverse to the yield in tension), the facilitating role of compression, and other observations lead to a peculiar conjecture [18]. The fracture and coalescence of nanocrystals can be performed reversibly, if little or none of the configurational entropy is produced in a slow enough cycle: While a tensile force causes necking and separation in two properly capped fragments, upon compression, these fragments can possibly be brought together and healed seamlessly.

Our calculations do not include van der Waals repulsion that must vanish within the first steps, when a single covalent-bonded unit forms, and therefore does not increase the total barrier. Experiments suggest that this repulsion, preceding the coalescence, can be overcome at suitable conditions (temperature, irradiation, pressure [4,6,12]). The feasibility of the SW flip is established, and its possible catalysis (by metal, carbon [10], and possibly hydrogen [6]) has been discussed. Experimentally, besides the improvement in properties of the CNT array or crystal, in a more challenging setup two CNTs can be brought in proximity by a scanning probe and forced to weld by thermal or electronic agitation [18]. It is feasible in such an arrangement to detect the useful behavior of the emerging quantum dot or heterojunction [e.g., a $(5,0)$ or $(5,5)$ neck between the $(10,10)$ "electrodes wires," (Fig. 2)].

In summary, we present for the first time atomically precise routes for complete coalescence of generic fullerene cages: cap-to-cap CNTs and C_{60} merging to form a defectless final structure. The entire process is reduced to a sequence of SW bond switches and therefore is likely the lowest energy path for transition. Several other examples of merging follow immediately as special cases: buckyballs in a peapod, or two $(5,5)$ tubes can repeat Fig. 1 exactly, welding of $(5,5)$ to $(10,10)$ follows Fig. 4, etc. The approach remains valid for arbitrary tubes with the important constraint of grain boundary for tubes of different chirality. The junction of (n,m) and (n',m') must contain $5/7$ dislocations or their equivalent of $(n-n',m-m')$ total Burgers vector [11]. The proposed mechanism has important implications for nanotube material (crystals, ropes) processing and property enhancement, engineering of nanoscale junctions of various types, possible CNT growth mechanisms with the C_{60} and other nanoparticles as feedstock.

This work was supported by AFOSR and Materials Directorate of the Air Force Research Laboratory, the Office of Naval Research DURINT grant, and the Nanoscale Science and Engineering Initiative of the NSF, No. EEC-0118007.

*Corresponding author.
Electronic address: biy@rice.edu

[1] R. P. Feynman, Eng. Sci. **23**, 22 (1960).
[2] D. J. Wales, M. A. Miller, and T. R. Walsh, Nature (London) **394**, 758 (1998); D. J. Wales and H. A. Scheraga, Science **285**, 1368 (1999).
[3] M. S. Dresselhaus, G. Dresselhaus, and P. C. Eklund, *Science of Fullerenes and Carbon Nanotubes* (Academic Press, San Diego, 1996).
[4] B. W. Smith, M. Monthioux, and D. E. Luzzi, Chem. Phys. Lett. **315**, 31 (1999); J. Sloan *et al.,* Chem. Phys. Lett. **316**, 191 (2000); S. Wang and P. R. Buseck, Chem. Phys. Lett. **182**, 1 (1991).
[5] D. L. Strout, R. L. Murry, C. Xu, W. C. Eckhoff, G. K. Odom, and G. E. Scuseria, Chem. Phys. Lett. **214**, 576 (1993); M. Terrones, H. Terrones, and W. K. Hsu, Chem. Soc. Rev. **24**, 341 (1995), and references therein; Y. Xia, Y. Xing, C. Tan, and L. Mei, Phys. Rev. B **53**, 13 871 (1996).
[6] P. Nikolaev, A. Thess, A. G. Rinzler, D. T. Colbert, and R. E. Smalley, Chem. Phys. Lett. **266**, 422 (1997); M. Terrones, H. Terrones, F. Banhart, J.-C. Charlier, and P. M. Ajayan, Science **288**, 1226 (2000).
[7] D. B. Geohegan *et al.,* Appl. Phys. Lett. **78**, 3307 (2001); see also R. E. Smalley, Nav. Res. Rev. **18**, 3 (1991).
[8] R. R. Schlittler *et al.,* Science **292**, 1136 (2001).
[9] M. Fujita, R. Saito, G. Dresselhaus, and M. S. Dresselhaus, Phys. Rev. B **45**, 13 834 (1992).
[10] B. R. Eggen, M. I. Heggie, G. Jungnickel, C. D. Latham, R. Jones, and P. R. Briddon, Science **272**, 87 (1996); G. E. Scuseria, Science **271**, 942 (1996); A. J. Stone and D. J. Wales, Chem. Phys. Lett. **128**, 501 (1986).
[11] B. I. Yakobson, Appl. Phys. Lett. **72**, 918 (1998); M. Buongiorno Nardelli, B. I. Yakobson, and J. Bernholc, Phys. Rev. Lett. **81**, 4656 (1998); H. F. Bettinger, T. Dumitrica, G. E. Scuseria, and B. I. Yakobson, Phys. Rev. B **65**, 041406 (2002); Ge. Samsonidze, Gu. Samsonidze, and B. I. Yakobson, Phys. Rev. Lett. **88**, 065501 (2002); B. I. Yakobson, U.S. Patent No. 6 280 677 B1 (2001).
[12] *Fullerene Polymers and Fullerene Polymer Composites,* edited by P. C. Eklund and A. M. Rao (Springer, Berlin, 2000); A. M. Rao *et al.,* Science **259**, 955 (1993).
[13] See AIP Document No. EPAPS: E-PRLTAO-88-039219 for full sequences corresponding to Figs. 2 and 4, animated as MPG files, together with the simulation of (10, 10) pair. This document may be retrieved via the EPAPS homepage (http://www.aip.org/pubservs/epaps.html) or from ftp.aip.org in the directory /epaps/. See the EPAPS homepage for more information.
[14] C. M. Goringe, D. R. Bowler, and E. Hernandez, Rep. Prog. Phys. **60**, 1447 (1997).
[15] M. J. Frisch *et al.,* GAUSSIAN 98, Revision A.6 (Gaussian, Inc., Pittsburgh, 1998).
[16] B. I. Yakobson, Ge. Samsonidze, and Gu. Samsonidze, Carbon **38**, 1675 (2000).
[17] J. Tersoff, Phys. Rev. B **37**, 6991 (1988); D. W. Brenner, Phys. Rev. B **42**, 9458 (1990).
[18] U. Landman, W. D. Luedtke, B. E. Salisbury, and R. L. Whetten, Phys. Rev. Lett. **77**, 1362 (1996); U. Landman, W. D. Luedtke, N. A. Bernham, and R. J. Colton, Science **248**, 454 (1990).